HHS Public Access

Author manuscript

Clin Cancer Res. Author manuscript; available in PMC 2020 December 01.

Published in final edited form as:

Clin Cancer Res. 2020 June 01; 26(11): 2573–2581. doi:10.1158/1078-0432.CCR-19-2897.

In-vivo tracking of adoptively transferred natural killer-cells in rhesus macaques using ^{89}Zirconium-oxine cell labeling and PET imaging

Noriko Sato[1], **Kate Stringaris**[2], **Jan K. Davidson-Moncada**[2,3], **Robert N. Reger**[2], **Stephen S. Adler**[4], **Cynthia E. Dunbar**[5], **Peter L. Choyke**[1,*], **Richard W. Childs**[2,*]

[1]Molecular Imaging Program, National Cancer Institute, National Institutes of Health, Bethesda, MD

[2]Cellular and Molecular Therapeutics Branch, National Heart, Lung, and Blood Institute, National Institutes of Health, Bethesda, MD.

[3]Center for Human Immunology, National Heart, Lung, and Blood Institute, National Institutes of Health, Bethesda, MD

[4]Clinical Research Directorate, Frederick National Laboratory for Cancer Research sponsored by the National Cancer Institute, Frederick, MD

[5]Translational Stem Cell Biology Branch, National Heart, Lung, and Blood Institute, National Institutes of Health, Bethesda, MD.

Abstract

Purpose: Trials of adoptive natural killer (NK)-cell immunotherapy for hematological malignancies have thus far shown only marginal effects, despite the potent *in-vitro* anti-tumor activity of these cells. Homing of infused cells to tumor microenvironments is critical for efficacy but has not been well characterized. We established a novel method to track and quantify the distribution of adoptively transferred NK-cells using rhesus macaques (RMs) as a clinically relevant preclinical model.

Experimental Design: RM NK-cells were expanded *ex-vivo* for 14–21 days, labeled with ^{89}Zr-oxine complex and assessed for phenotype, function and survival. Trafficking of ^{89}Zr-labeled *ex-vivo*-expanded NK-cells infused into RMs was monitored and quantitated by serial positron emission tomography (PET)/computed tomography (CT) (n=3, 2.05 ± 0.72 MBq, 23.5 ± 2.0×10^6 NK-cells/kg) and compared to that of ^{89}Zr-labeled non-expanded NK-cells, apoptotic NK-cells and hematopoietic stem and progenitor cells (HSPCs).

Correspondence: Noriko Sato, M.D., Ph.D., Molecular Imaging Program, National Cancer Institute, National Institutes of Health, Bethesda, MD 20892; Phone; 240-858-3079, fax number; 240-541-4526, saton@mail.nih.gov.

Author Contributions

N.S., P.L.C. and R.W.C. conceived and designed the study. N.S. and J.K.D.-M. deloped the method. N.S., K.S., J.K.D.-M. R.N.R. and S.S.A. acquired and analyzed the data. N.S., K.S., S.S.A., C.E.D., P.L.C. and R.W.C. performed data interpretation. N.S. wrote and N.S., K.S., C.E.D., P.L.C. and R.W.C. revised the manuscript. All authors reviewed and approved the manuscript.

*Contributed equally to this study.

Conflict of interest: The authors declare no competing financial interests. The authors N.S. and P.L.C. have filed U.S. Patent Applications for generation and application of the ^{89}Zr-oxine complex. The author R.W.C. has filed a U.S. Patent Application for the method used in this study to expand NK-cells *ex-vivo*.

Results: NK-cells retained sufficient levels of ^{89}Zr for accurate *in-vivo* tracking for 7 days. ^{89}Zr-labeling did not alter cellular phenotype, viability or function. PET/CT showed NK-cells initially localized in the lungs, followed by their migration to the liver, spleen and, at low levels, bone marrow (BM). One day following transfer, only 3.4% of infused NK-cells localized to the BM vs 22.1% of HSPCs. No clinical side effects were observed, and dosimetry analysis indicated low organ radio-exposures of 6.24 mSv/MBq (spleen) or lower.

Conclusions: These data support translation of this technique to humans to track the distribution of adoptively infused cells and to develop novel techniques to improve immune cell homing to tumor microenvironments.

Keywords

Natural killer cells; Cell tracking; Positron emission tomography; Zirconium-89; Rhesus macaque

Introduction

Adoptive-transfer of allogeneic and autologous NK-cells is being investigated clinically for the treatment of malignancies. Despite their capacity to induce cellular cytotoxicity, NK-cells maintain self-tolerance regulated by the interaction of activating and inhibitory receptors with self-MHC class I molecules and their derivatives (1–4). The lack of a requirement for prior sensitization and the ability to induce tumor cytotoxicity in an antigen-independent manner without causing graft-versus-host disease (5) may offer advantages to adoptive NK-cell immunotherapy compared to approaches using T-cells. Although regression of malignancies in humans with advanced cancers has been observed, overall efficacy of NK-cell based immunotherapy remains marginal (6–8). One potential limitation of adoptive NK-cell therapy for leukemia and other hematological malignancies may be the inability of NK-cells to efficiently traffick to bone marrow (BM) where these malignancies primarily reside (9,10). Most preclinical adoptive NK-cell studies have used tissue harvesting to identify transferred cells. Such approaches preclude longitudinal analysis of cell fate and are problematic in humans.

Imaging adoptively transferred cells *in-vivo* could provide a useful method to assess the capacity of NK-cell homing to desired locations, such as tumors. Among the cell tracking imaging methods clinically available, magnetic resonance imaging (MRI) with *ex-vivo* superparamagnetic iron oxides (SPIOs) cell labeling permits high resolution without ionizing radiation, however, interpretation and quantitation are difficult and the SPIOs remain in the tissue after labeled-cell death (11). Indium-111 (^{111}In)-oxine for single-photon emission computed tomography imaging has been used to label hematopoietic cells, but the high ^{111}In doses required can impair cellular viability and function (12,13).

A ^{89}Zr-oxine complex was recently developed as a cell labeling agent for tracking cells utilizing positron emission tomography (PET) (14). ^{89}Zr has a half-life of 78.4 hours, ideal for tracking labeled cells over multiple days. With inherently higher sensitivity and spatial resolution of PET (15), studies in various murine models have established that only extremely low doses of ^{89}Zr-oxine are necessary to track labeled cells for up to 7 days, with minimal to no deleterious radio-toxicity (14,16,17).

Here, we present a method to track adoptively transferred *ex-vivo*-expanded NK-cells using ^{89}Zr-oxine cell labeling and PET imaging, validated *in-vivo* in a clinically relevant large animal model using rhesus macaques (RMs). Tissue ^{89}Zr-distribution accurately quantitated NK-cell trafficking with low radio-exposure to organs, suggesting this method can be safely translated to humans.

Materials and methods

Animal care

All RM experiments were performed in accordance with a protocol approved by the institutional animal care and use committee. RMs were monitored daily in an Association for Assessment and Accreditation of Laboratory Animal Care International-approved facility.

Collection and purification of NK-cells and expansion

See Supplementary Methods for material sources and details. Briefly, RM or human NK-cells were first enriched by either a) T-cell depletion of peripheral blood mononuclear cells (PBMCs) alone or b) additional NK-cell selection with NKp80 for RM or CD56 for human NK-cells. Enriched NK-cells were then expanded for 14–21 days as per an ongoing clinical trial of adoptive NK-cell therapy (NCT00720785) (18,19), by co-culturing with an irradiated (100 Gy) human Epstein-Barr virus transformed lymphoblastoid cell line (SMI-EBV-LCL, authenticated 3/4/2009 by The Center for Cell and Gene Therapy using HLA typing) in X-VIVO 20 medium with 10% RM or human serum, supplemented with 500 IU/ml recombinant human interleukin (IL)-2. For experiments using non-expanded RM NK-cells, PBMCs obtained by apheresis and density-gradient centrifugation (Ficoll, GE Healthcare) were magnetically depleted of $CD3^+$ (T-cells), $CD20^+$ (B-cells), and $CD14^+$ cells (monocytes), before positive-selection of NK-cells with anti-NKp80, a marker present on the vast majority of RM NK-cells, in contrast to CD56, which is downregulated in a population of mature NK-cells in RM (20).

Collection and purification of hematopoietic stem and progenitor cells

RM $CD34^+$ hematopoietic stem and progenitor cells (HSPCs) were purified as described following mobilization with granulocyte-colony stimulating factor and plerixafor, apheresis and then immunomagnetic selection (21,22) (Supplementary Methods). Eight million $CD34^+$ HSPCs with a purity of 92.3% were isolated and labeled with ^{89}Zr-oxine prior to PET/CT studies.

Synthesis of ^{89}Zr-oxine complex and cell labeling.

^{89}Zr-oxine complex was synthesized from $^{89}ZrCl_4$ produced at the institutional cyclotron facility (23) and oxine, as previously reported (14,16). RM or human NK-cells in phosphate-buffered saline (PBS) were incubated with ^{89}Zr-oxine solution (63–100 kBq/10^6 cells) at a 30:1 volume ratio for 15 minutes, washed twice in the culture medium and transferred to a new tube in culture medium for *in-vitro* assays or in PBS for PET/CT studies. $CD34^+$ HSPCs were labeled in a similar manner.

Impact of ^{89}Zr-labeling on NK-cell surface phenotype, viability, function, and ^{89}Zr-activity retention

NK-cells with and without ^{89}Zr-oxine labeling were cultured in medium without IL-2 and, at indicated time points, examined for CD16, CD56, NKG2A, annexin V, Ki67 and CD107a expression by flow cytometry (FACSCalibur or LSRII, BD Biosciences) or assessed for cell number and ^{89}Zr-activity retention (see Supplementary Methods for antibody and reagent information and details). Ki67 staining was performed using the cells fixed and permeabilized with −20°C 80% ethanol. To evaluate degranulation, a surrogate for cytotoxic function, at each time point, 5×10^6 NK-cells were co-cultured with 5×10^6 K562 target cells (human chronic myeloid leukemia in blast crisis) purchased from American Type Culture Collection (ATCC, authenticated on 3/8/2019 by ATCC using short-tandem repeat profiling) for 3 hours and NK-cell CD107a expression was analyzed. Viable cell quantitation was performed using 0.4% trypan blue dye (Thermo Fisher Scientific). The cell suspension was spun, and ^{89}Zr-activity of the pellet was measured by a γ-counter (γ-WIZARD2, Perkin Elmer) and corrected for ^{89}Zr-activity decay.

Assessing whether ^{89}Zr transferred from ^{89}Zr-oxine-labeled NK-cells to neighboring cells

^{89}Zr-oxine-labeled human NK-cells from healthy donors were cultured alone or with different cell types (non-^{89}Zr-labeled) for 24–36 hours. Thereafter, the two cell types were dissociated by magnetic separation and ^{89}Zr-activity was measured for each population (Supplementary Methods).

Tracking cells by a clinical PET/CT imager

Supplementary Table S1 summarizes the ^{89}Zr-oxine-labeled cell doses infused to RMs in this study. All RMs (weight 6.4 ± 0.9 kg) received a continuous intravenous infusion of deferoxamine (Desferal) beginning immediately before ^{89}Zr-oxine-labeled cell transfer until day 7, using first a 15 mg/kg/hour loading dose for 4 hours then 3 mg/kg/hour for the remainder of the study. RMs underwent serial PET/CT imaging for up to 7 days using a clinical PET/CT scanner (Supplementary Methods). In addition to autologous, *ex-vivo*-expanded NK-cells, 3 RMs served as controls to track 3 alternative autologous cell populations; a) non-expanded NK-cells, b) apoptotic NK-cells, and c) HSPCs. VivoQuant software (inviCRO LLC) was used to fuse the maximum intensity projection (MIP) PET images with CT.

Quantitation of PET images

To quantitate ^{89}Zr distribution, contours were drawn on the acquired PET/CT images delineating organs and whole-body using MIMvista (MIM software). Standardized uptake value (SUV) was calculated by the formula: SUV = [Bq/ml (decay corrected) in tissue] / [Bq of the cells injected/body weight (grams)]. Percentage of injected dose (% ID) was calculated by decay corrected activity in the tissue divided by the injected dose.

Dosimetry

Dosimetry estimates were derived using the organs showing high ^{89}Zr-activity from which residence times were measured. The residence times were converted to human equivalent

and used as input parameters into OLINDA 1.1 (Vanderbilt University). See Supplementary Methods.

Liver biopsy

Expanded autologous RM NK-cells were labeled with 2 μM CellTracker Orange CMRA (Thermo Fisher Scientific) according to the manufacturer's instructions, then intravenously infused into the RM (5×10^7 cells/kg). One day later, a percutaneous liver biopsy was performed under anesthesia. The fresh biopsy samples were analyzed using an inverted Leica SP5 five-channel confocal multiphoton microscope (Leica Microsystems), employing 561-nm excitation and 570–640nm emission range (Supplementary Methods). Flow cytometry analysis (Fortessa, BD Biosciences) was also performed on liver tissue mashed into suspension and stained with aqua live/dead stain (Thermo Fisher Scientific).

Statistical analysis

NKG2A expression was analyzed by Wilcoxon test. CD56/CD16 and CD107a expression within each time point, and expression of annexin V and Ki67 as well as cellular viability over time, were analyzed by repeated measure ANOVA with Sidak's test. Friedman test with Dunn's correction was used to compare CD107a expression at multiple time points. ^{89}Zr transfer from ^{89}Zr-labeled NK-cells to CD19$^+$ cells or PBMCs was analyzed by Wilcoxon test. Prism ver.8.2.0 (GraphPad Software) was used for all statistical analyses. The results are indicated as mean ± standard deviation (s.d.) and p-values less than 0.05 were considered significant.

Results

^{89}Zr-oxine labeling does not alter the phenotype, viability nor function of expanded NK-cells

We first examined whether labeling RM and human NK-cells with ^{89}Zr-oxine complex had any impact on NK-cell phenotype. RM and human NK-cells labeled at 19.5 ± 4.0 kBq/10^6 cells and 20.2 ± 4.0 kBq/10^6 cells, respectively, were used in all *in-vitro* experiments. Flow cytometry analysis indicated that expression of CD56 and CD16 (RM: n=9, human: n=7), and NKG2A (RM: n=8), was not altered immediately (3 hours) after ^{89}Zr-oxine labeling (Fig. 1A and B) or over the subsequent 24 hours of culture (n=3, Supplementary Fig. S1). These conditions were chosen to mimic an *in-vivo* environment in patients not receiving exogenous IL-2.

We next assessed the viability of labeled cells and retention of ^{89}Zr. ^{89}Zr-oxine-labeled and non-labeled RM NK-cells showed similar viability and similar decline in live cell number (Fig. 1C, n=11) over time, as well as a similar increase in the percentage of the annexin V$^+$ apoptotic/necrotic cells (Fig. 1D, n=3). Some cells proliferated at early time points, as indicated by Ki67 expression, which is likely due to ligering effect of IL-2 used for *ex-vivo* expansion (Fig. 1D, n=3). As a result, ^{89}Zr-radioactivity per cell declined to approximately 50% of initial ^{89}Zr-activity by day 3 (Fig. 1E, n=6). Similar findings were observed with human NK-cells (Fig. 1F: n=9, G: n=3, H: n=6). ^{89}Zr labeling did not impair the cytotoxic function of RM (Fig. 1I, n=3) or human (Fig 1J, n=3) NK-cells; degranulation, assessed by

measuring NK-cell surface CD107a expression up to 24 hours following co-culture with K562 tumor cells, was similar between ^{89}Zr-labeled and non-labeled NK-cells.

^{89}Zr is not readily transferred from the labeled NK-cells to neighboring cells

To exclude the possibility that ^{89}Zr could transfer from labeled to non-labeled cells *in-vivo*, which would confound the interpretation of ^{89}Zr signals on PET/CT, we assessed whether ^{89}Zr could be transferred from labeled NK-cells to adjacent cells *ex-vivo* by passive diffusion. When ^{89}Zr-oxine-labeled human NK-cells were co-cultured with Raji or Ramos cells for 24–36 hours, >96% of ^{89}Zr-activity remained within the NK-cells after re-purification of the co-cultured cells (Fig. 1K, n=3). More importantly, the radioactivity detected in the CD19^{+} fraction (either Raji or Ramos cells) did not differ from background radioactivity measured when a sham CD19^{+} cell selection was performed on ^{89}Zr-labeled NK-cells alone. Similar results were found when NK-cells from 3 HLA-A2 negative donors were labeled with ^{89}Zr-oxine and co-cultured with HLA-A2 positive PBMCs. The ^{89}Zr-activity in the immunomagnetically-selected HLA-A2 positive fraction was equivalent to the background radioactivity obtained from a sham HLA-A2 positive selection of ^{89}Zr-labeled HLA-A2 negative NK-cells alone (Fig. 1L, n=3). These data suggest that ^{89}Zr-oxine-labeled NK-cells retain the radiolabel without significant transfer to neighboring cells.

PET/CT imaging provides clear visualization of the trafficking of adoptively transferred ^{89}Zr-oxine-labeled NK-cells in RMs.

Sequential PET/CT imaging of autologously-transferred ^{89}Zr-oxine-labeled expanded NK-cells (n=3, 2.05 ± 0.72 MBq, 13.6 ± 5.3 kBq/10^6 cells, 23.5 ± 2.0×10^6 NK-cells/kg, Supplementary Table S1) showed initial localization to the lungs, followed by migration to the liver and spleen (Fig. 2A). The majority of NK-cells remained in these organs until day 7, when the experiment concluded. ^{89}Zr-accumulation in the bladder indicates effective renal clearance of free ^{89}Zr by deferoxamine. Low levels of radioactivity were observed within the BM, as shown in an axial PET/CT section of the 4th lumber vertebrae with ^{89}Zr-activity localized in the center of the spinal body, the location of vertebral marrow (Fig. 2B). In contrast, measurable labeled NK-cells were not localized within lymph nodes. Quantitation of organ ^{89}Zr-activity on acquired images showed the SUV of the liver and spleen reached an average of 14.4 and 25.3 respectively on day 1, in contrast to the BM which only reached an SUV of 0.64 (Fig. 2C and Supplementary Fig. S2A which shows the same data with magnification of the X-axis up to day 1). The percentage of ^{89}Zr-activity measured in the liver corresponded to 31.3 ± 8.1% and 34.7 ± 11.8% of the infused ^{89}Zr-activity on days 1 and 2 respectively, indicating that approximately one third of the transferred cells had trafficked to the liver (Fig. 2D and Supplementary Fig. S2B for magnification up to day 1). In contrast, only approximately 3% of the cells homed to the spleen and BM at these time points. As expected, whole-body radioactivity declined over time (Fig. 2E), likely due to renal clearance of ^{89}Zr released from dead cells and chelated by deferoxamine, suggesting that one third and one half of the transferred *ex-vivo*-expanded NK-cells had died by days 2 and 7, respectively.

Deferoxamine infusion results in rapid renal clearance of ^{89}Zr released from apoptotic NK-cells

It is well documented that free ^{89}Zr can be taken up by bone (24). Our previous study in mice using ^{89}Zr-labeled cells demonstrated that deferoxamine infusion can prevent bone uptake of free ^{89}Zr (16). To confirm that continuous infusion of deferoxamine efficiently bound and then excreted free ^{89}Zr released from dead cells in RM and that the ^{89}Zr-signals observed in Fig. 2A are from live cells, we performed a cell tracking study using *ex-vivo*-expanded NK-cells that had become apoptotic as a consequence of removing IL-2 from the medium used to culture cells *ex-vivo* (276 kBq, 15 kBq/10^6 cells, 3.5×10^6 cells/kg, Supplementary Table S1). In contrast to RMs receiving viable NK-cells, we observed significant radioactivity in the kidneys and bladder when the initial scan (20 minutes duration) was conducted (Fig. 3A) following the apoptotic NK-cell transfer, consistent with rapid renal clearance of ^{89}Zr. Although some ^{89}Zr-labeled apoptotic NK-cells were initially observed in the lungs and liver, by 4 hours, virtually all the ^{89}Zr had moved to the bladder. On day 1, only 8.3 % of the total administered ^{89}Zr remained in the body. These data show that deferoxamine chelation is effective in preventing transfer of free ^{89}Zr from dying and/or dead cells into bone or other cellular populations with phagocytic capacity. Of note, following the infusion of apoptotic cells, a small amount of ^{89}Zr accumulated in the gallbladder (1.5% ID at 4 hours), suggesting low-level clearance of ^{89}Zr via the liver into the gallbladder.

Both freshly isolated and *ex-vivo*-expanded NK-cells showed limited BM homing compared to HSPCs

To assess whether *ex-vivo*-expansion may have altered the homing profile of NK-cells, the same ^{89}Zr-oxine labeling and PET/CT approach was employed using non-expanded RM NK-cells (185 kBq, 6.9 kBq/10^6 cells, 4.0×10^6 cells/kg, Supplementary Table S1). The cell number (and therefore ^{89}Zr-activity) infused was low because the number of NK-cells obtainable by purification from blood, without expansion, was limited. Compared to expanded NK-cells (Fig. 4A), non-expanded NK-cells distributed slightly less to liver and more to spleen, but their relative homing to the BM appeared similarly low (Fig. 4B). For comparison, we tracked ^{89}Zr-oxine-labeled CD34$^+$ HSPCs, a cell population known to efficiently localize and engraft in the BM (355 kBq, 44.4 kBq/10^6 cells, 1.2×10^6 cells/kg, Supplementary Table S1). In contrast to NK-cells, HSPCs showed robust trafficking to the BM, although infused cell number and ^{89}Zr-activity were also low due to the limitation imposed by the number of these rare cells available for labeling (Fig. 4C, Supplementary S3A). The BM % ID on day 1 for expanded NK-cells, non-expanded NK-cells and HSPCs were 3.4%, 2.4% and 22.1%, respectively (Fig. 4D, Supplementary Fig. S3B). These results show labeled HSPCs can still home to BM and validate the sensitivity of this approach for tracking cell populations of interest to the BM. Importantly, they show that only a small fraction of adoptively transferred NK-cells trafficked to BM, suggesting the capability of infused NK-cells to home to normal BM is limited.

Liver biopsy shows presence of transferred NK-cells in the liver

To confirm that the radioactivity detected in the liver by PET/CT following the infusion of ^{89}Zr-oxine-labeled NK-cells (Fig. 2A) reflected viable NK-cells that had homed to this organ, a liver biopsy was performed 24 hours following the infusion of CMRA-labeled NK-cells (Fig. 5A). Microscopic analysis of the collected samples showed CMRA-labeled NK-cells residing in the liver (Fig. 5B). Furthermore, flow cytometry analysis of the biopsy sample confirmed the presence of viable CMRA-positive NK-cells within the liver ($CD56^+$ NK-cells represented 0.29 % of the liver lymphocyte population, Fig. 5C).

Safety profile of ^{89}Zr-oxine-labeled NK-cell PET suggests this study approach is translatable to humans.

RMs did not have any changes in their vital signs, weight or clinical exam following the infusion of ^{89}Zr-oxine-labeled cells. Dosimetry in humans, extrapolated from distribution of ^{89}Zr-labeled NK-cells in RMs, indicated that the highest radio-exposure was observed in the spleen and liver (6.24 and 3.88 mSv/MBq, respectively, Table 1). When considering the U.S. Nuclear Regulatory Commission safety guideline limits of 500 mSv per organ or 50 mSv total body, per year, our data suggest that ^{89}Zr-labeled NK-cells below 80.1 MBq (2.17 mCi)/70 kg doses [*i.e.* 1.14 MBq (30.9 μCi)/kg doses] per year could be infused safely into humans while allowing for tracking of the cells to locations of interest.

Discussion

Although pilot trials have established that adoptive NK-cell transfer can induce anti-tumor effects, the overall efficacy to date of NK-cell-based immunotherapy has been limited (6–8). One reason may be that infused NK-cells are simply not migrating through the blood stream to relevant target organs where the malignancies reside, such as the BM or lymph nodes for hematological malignancies. In this study, we developed a method of tracking NK-cells *in-vivo* using ^{89}Zr-oxine *ex-vivo* cell labeling and PET/CT imaging in RM. RM NK-cells have similar phenotypic and functional properties to human NK-cells and can be expanded *ex-vivo* using methods currently utilized in clinical trials (20). In contrast, mouse NK-cells have significant phenotypic and functional divergence from human NK-cells. For instance, most mouse NK-cells lack Fas and TNF-related apoptosis-inducing ligand used to kill tumor targets (25,26), and they do not possess killer-cell immunoglobulin-like receptors (27,28) which play a critical role in regulating NK-cell cytotoxicity. Further, most conditions used for expanding human NK-cells *ex-vivo* are ineffective in expanding murine NK-cells. Taken altogether, these factors favor the use of RMs over mice for studies exploring NK-cell trafficking.

The BM is the site of origin and proliferation of many hematological malignancies. NK-cells are known to express BM homing receptors such as CXCR4 (29) and CD62L (30). However, CXCR4 may be downregulated during *ex-vivo* NK-cell expansion (29,30) and E-selectin ligands expressed on expanded NK-cells are primarily non-glycosylated, making them inactive for binding E-selectin which is expressed on BM endothelial cells (31). These, as well as other factors, may in part account for the limited BM trafficking of *ex-vivo*-expanded NK-cells that we observed in our study. However, it is important to consider that we also

observed that non-expanded NK-cells had poor homing to the BM. Migration of NK-cells to lymph nodes was also not observed, consistent with low expression and/or down-regulation of CCR7 reported during culture (32). In contrast, as would be expected, ^{89}Zr-oxine-labeled HSPCs showed robust trafficking to the BM. Collectively, the low level trafficking observed with adoptively transferred NK-cells to the BM of RMs may in part explain the limited efficacy observed in clinical trials exploring adoptive NK-cell therapy for BM malignancies. It is possible that NK-cells would show superior homing or may only home to the bone marrow infiltrated by malignant cells. Unfortunately, we lack primate models for hematological malignancies to address this interesting question.

We observed high levels of liver homing of transferred NK-cells. Recent studies have revealed that high numbers of NK-cells, consisting of 30–40% lymphocytes, reside in the liver (33). Attraction and retention of NK-cells in the liver are considered to be mediated by chemokines such as CCL3, CCL5, and CXCL16, but only the CD56^{bright} hepatic NK-cells have been characterized to express receptors for these ligands (34,35). In the context of our study's findings, a characterization of liver homing receptors on NK-cells expanded using a variety of different approaches would be of interest. Modification of expansion conditions (9,10) or genetic modification of NK-cells to over-express BM homing receptors (29) or to under-express liver homing receptors may improve trafficking of these cells to the BM. ^{89}Zr-oxine cell tracking could be a very useful tool to assess the impact of such maneuvers to alter NK-cell homing to the BM, lymph nodes, and other target tissues.

Previous studies suggest that, following ^{89}Zr-oxine cell membrane permeabilization, ^{89}Zr is retained in viable cells (14,16). Cell survival in culture showed substantial donor-to-donor variation, likely accounting for the large standard deviations observed in the calculated ^{89}Zr-activity per cell. Further, following harvesting of *ex-vivo*-expanded NK-cells, some degree of proliferation continued to occur even after cells were labeled with ^{89}Zr-oxine. We believe this persisting NK-cell proliferation likely caused the decline of ^{89}Zr-activity/cell observed at earlier time points. In this context, ^{89}Zr-oxine-labeled cells that are damaged or die following adoptive-transfer would be expected to release free ^{89}Zr. Whole body ^{89}Zr retention after labeled-NK-cell transfer was higher than expected from extrapolation of *in-vitro* retention over time. Better *in-vivo* survival of NK-cells could perhaps be explained by support from endogenous cytokines such as IL-15, or microenvironmental survival signals provided by tissues.

Although the majority of released ^{89}Zr is excreted via the kidneys (14), it is possible that a fraction of free ^{89}Zr could bind to hydroxyapatite in bone resulting in high ^{89}Zr-signals in the bones (24), potentially confounding the accurate quantitation of cellular homing to the BM. To preclude this possibility in our experiments, RMs received a continuous infusion of deferoxamine, the most commonly used and clinically applicable chelator for ^{89}Zr (36), to chelate and promote the renal excretion of any free ^{89}Zr. In our previous murine studies, multiple intramuscular injections of deferoxamine reduced bone uptake of free ^{89}Zr (14,16). As RM studies are limited by regulations and availability, it was not feasible to perform control ^{89}Zr-oxine labeled NK-cell tracking in the absence of deferoxamine. Although bone uptake of ^{89}Zr would spuriously inflate calculated marrow localization, the very low BM

localization observed with ^{89}Zr-labeled NK-cells in our study does not confound our conclusions.

The experiment infusing ^{89}Zr-labeled apoptotic NK-cells, confirmed the efficiency of deferoxamine chelation and suggests that deferoxamine minimizes the direct transfer of ^{89}Zr from dead/dying cells to phagocytes. Of note, *in-vitro* experiments did not detect ^{89}Zr transfer from live ^{89}Zr-oxine-labeled NK-cells to non-labeled cells when two cell populations were co-cultured, including PBMCs containing cells with phagocytic properties. These characteristics of ^{89}Zr-retention within live cells and release and rapid clearance of ^{89}Zr from the circulation after cell death are essential for accurate interpretation of imaging studies using radiolabeled agents for *in-vivo* cell tracking. Importantly, liver biopsy revealed that viable CMRA-labeled NK-cells were present in a RM following adoptive infusion of NK-cells, confirming the findings of the PET studies. Further, the deferoxamine doses we used were the same as those administered to humans treated with this agent for iron overload, establishing the clinical applicability of this strategy for patients receiving ^{89}Zr-oxine-labeled NK-cells.

The PET studies provided a good dosimetry model to estimate potential radio-exposure in humans. The spleen and liver received the highest exposure among organs, however, the doses were still well within safety guidelines when no more than 157.7 MBq (4.26 mCi)/70 kg doses (*i.e.* 1.14 MBq (30.9 μCi)/kg doses) are administered to humans. This corresponds to 83.8×10^6 NK-cells/kg when the cells were labeled with a specific activity of 13.6 kBq/10^6 cells used in this study. We observed high background noise with the PET/CT images of non-expanded NK-cells when only 185 kBq (27.2 kBq/kg) was infused, due to the small number of NK-cells we were able to purify from PBMCs, suggesting this dose is at the detection limit of PET/CT. On the other hand, the dose used for HSPCs (355 kBq, 54.6 kBq/kg) generated high quality images with low background noise. Based on these results, we estimate that an approximately 55 kBq (1.5 μCi)/kg dose of ^{89}Zr-oxine-labeled cells would be sufficient to provide good quality images by PET/CT to accurately track these cells *in-vivo*. These data indicate that in future clinical trials evaluating adoptive NK-cell infusions in humans, where cell numbers in the order of $5–10\times10^8$ cells/kg are typically infused, only a small fraction of the cells being infused would need to be labeled to provide robust qualitative and quantitative information on cellular trafficking.

In conclusion, ^{89}Zr-oxine labeling of NK-cells followed by PET/CT imaging represents a promising new tool to track the *in-vivo* fate of adoptively transferred NK-cells. The RM model presented here provides a method to evaluate and optimize various strategies to improve NK-cell trafficking and homing to the BM, lymph nodes, and other locations where hematological malignancies and tumors reside. These preclinical *in-vitro* and *in-vivo* data suggest this technology could be safely extended to humans and could be applied to other cellular populations besides NK-cells.

Supplementary Material

Refer to Web version on PubMed Central for supplementary material.

Acknowledgements

We thank Marvin L Thomas, Theresa M. Engels, Randall R. Clevenger, Timothy Hunt, Kenneth R. Jeffreys, Mark Metzger, Allen E. Krouse, Sandra D. Price, Robert E. Donahue, Robert F. Hoyt, Jr., Karen J. Keeran, Arthur Zetts and Shawn Kozlov for animal care, Lawrence P. Szajek for generating $^{89}ZrCl_4$, and Gideon K. Kwarteng, Philip C. Eclarinal and Alicia Forest for acquiring PET/CT, and Daniela A. Malide for microscopic analysis of the biopsy samples. We also wish to acknowledge the NHLBI and NCI intramural research programs, and the Dean R. O'Neill and Edward Rancic Cancer Fellowship for their support of this research.

Financial support: This research was supported by the Intramural Research Program of the National Institutes of Health, National Cancer Institute, Center for Cancer Research and the National Heart, Lung, and Blood Institute, Division of Intramural Research. Regarding S. Adler; This project has been funded in whole or in part with federal funds from the National Cancer Institute, National Institutes of Health, under Contract No. HHSN261200800001E. The content of this publication does not necessarily reflect the views or policies of the Department of Health and Human Services, nor does mention of trade names, commercial products, or organizations imply endorsement by the U.S. Government.

References

1. Farag SS, Caligiuri MA. Human natural killer cell development and biology. Blood Rev 2006;20(3):123–37 doi 10.1016/j.blre.2005.10.001. [PubMed: 16364519]
2. Caligiuri MA. Human natural killer cells. Blood 2008;112(3):461–9 doi 10.1182/blood-2007-09-077438. [PubMed: 18650461]
3. Vivier E, Raulet DH, Moretta A, Caligiuri MA, Zitvogel L, Lanier LL, et al. Innate or adaptive immunity? The example of natural killer cells. Science 2011;331(6013):44–9 doi 10.1126/science.1198687. [PubMed: 21212348]
4. Bern MD, Parikh BA, Yang L, Beckman DL, Poursine-Laurent J, Yokoyama WM. Inducible down-regulation of MHC class I results in natural killer cell tolerance. The Journal of experimental medicine 2019;216(1):99–116 doi 10.1084/jem.20181076. [PubMed: 30559128]
5. Ruggeri L, Aversa F, Martelli MF, Velardi A. Allogeneic hematopoietic transplantation and natural killer cell recognition of missing self. Immunol Rev 2006;214:202–18 doi 10.1111/j.1600-065X.2006.00455.x. [PubMed: 17100886]
6. Bjorklund AT, Carlsten M, Sohlberg E, Liu LL, Clancy T, Karimi M, et al. Complete Remission with Reduction of High-Risk Clones following Haploidentical NK-Cell Therapy against MDS and AML. Clinical cancer research : an official journal of the American Association for Cancer Research 2018;24(8):1834–44 doi 10.1158/1078-0432.CCR-17-3196.
7. Rubnitz JE, Inaba H, Ribeiro RC, Pounds S, Rooney B, Bell T, et al. NKAML: a pilot study to determine the safety and feasibility of haploidentical natural killer cell transplantation in childhood acute myeloid leukemia. J Clin Oncol 2010;28(6):955–9 doi 10.1200/JCO.2009.24.4590. [PubMed: 20085940]
8. Geller MA, Cooley S, Judson PL, Ghebre R, Carson LF, Argenta PA, et al. A phase II study of allogeneic natural killer cell therapy to treat patients with recurrent ovarian and breast cancer. Cytotherapy 2011;13(1):98–107 doi 10.3109/14653249.2010.515582. [PubMed: 20849361]
9. Miller JS, Rooney CM, Curtsinger J, McElmurry R, McCullar V, Verneris MR, et al. Expansion and homing of adoptively transferred human natural killer cells in immunodeficient mice varies with product preparation and in vivo cytokine administration: implications for clinical therapy. Biology of blood and marrow transplantation : journal of the American Society for Blood and Marrow Transplantation 2014;20(8):1252–7 doi 10.1016/j.bbmt.2014.05.004.
10. Grzywacz B, Moench L, McKenna D Jr., Tessier KM, Bachanova V, Cooley S, et al. Natural Killer Cell Homing and Persistence in the Bone Marrow After Adoptive Immunotherapy Correlates With Better Leukemia Control. Journal of immunotherapy (Hagerstown, Md : 1997) 2019;42(2):65–72 doi 10.1097/cji.0000000000000250.
11. Cianciaruso C, Pagani A, Martelli C, Bacigaluppi M, Squadrito ML, Lo Dico A, et al. Cellular magnetic resonance with iron oxide nanoparticles: long-term persistence of SPIO signal in the CNS after transplanted cell death. Nanomedicine (Lond) 2014;9(10):1457–74 doi 10.2217/nnm.14.84. [PubMed: 24823433]

12. Gholamrezanezhad A, Mirpour S, Ardekani JM, Bagheri M, Alimoghadam K, Yarmand S, et al. Cytotoxicity of 111In-oxine on mesenchymal stem cells: a time-dependent adverse effect. Nuclear medicine communications 2009;30(3):210–6 doi 10.1097/MNM.0b013e328318b328. [PubMed: 19262283]

13. Gildehaus FJ, Haasters F, Drosse I, Wagner E, Zach C, Mutschler W, et al. Impact of indium-111 oxine labelling on viability of human mesenchymal stem cells in vitro, and 3D cell-tracking using SPECT/CT in vivo. Molecular imaging and biology : MIB : the official publication of the Academy of Molecular Imaging 2011;13(6):1204–14 doi 10.1007/s11307-010-0439-1. [PubMed: 21080231]

14. Sato N, Wu H, Asiedu KO, Szajek LP, Griffiths GL, Choyke PL. (89)Zr-Oxine Complex PET Cell Imaging in Monitoring Cell-based Therapies. Radiology 2015;275(2):490–500 doi 10.1148/radiol.15142849. [PubMed: 25706654]

15. Rahmim A, Zaidi H. PET versus SPECT: strengths, limitations and challenges. Nuclear medicine communications 2008;29(3):193–207 doi 10.1097/MNM.0b013e3282f3a515. [PubMed: 18349789]

16. Asiedu KO, Koyasu S, Szajek LP, Choyke PL, Sato N. Bone Marrow Cell Trafficking Analyzed by (89)Zr-oxine Positron Emission Tomography in a Murine Transplantation Model. Clinical cancer research : an official journal of the American Association for Cancer Research 2017;23(11):2759–68 doi 10.1158/1078-0432.Ccr-16-1561. [PubMed: 27965305]

17. Asiedu KO, Ferdousi M, Ton PT, Adler SS, Choyke PL, Sato N. Bone marrow cell homing to sites of acute tibial fracture: (89)Zr-oxine cell labeling with positron emission tomographic imaging in a mouse model. EJNMMI Res 2018;8(1):109 doi 10.1186/s13550-018-0463-8. [PubMed: 30547233]

18. Berg M, Lundqvist A, McCoy P Jr., Samsel L, Fan Y, Tawab A, et al. Clinical-grade ex vivo-expanded human natural killer cells up-regulate activating receptors and death receptor ligands and have enhanced cytolytic activity against tumor cells. Cytotherapy 2009;11(3):341–55 doi 10.1080/14653240902807034. [PubMed: 19308771]

19. Childs RW, Berg M. Bringing natural killer cells to the clinic: ex vivo manipulation. Hematology Am Soc Hematol Educ Program 2013;2013:234–46 doi 10.1182/asheducation-2013.1.234. [PubMed: 24319186]

20. Hong HS, Rajakumar PA, Billingsley JM, Reeves RK, Johnson RP. No monkey business: why studying NK cells in non-human primates pays off. Front Immunol 2013;4:32 doi 10.3389/fimmu.2013.00032. [PubMed: 23423644]

21. Uchida N, Bonifacino A, Krouse AE, Metzger ME, Csako G, Lee-Stroka A, et al. Accelerated lymphocyte reconstitution and long-term recovery after transplantation of lentiviral-transduced rhesus CD34+ cells mobilized by G-CSF and plerixafor. Exp Hematol 2011;39(7):795–805 doi 10.1016/j.exphem.2011.04.002. [PubMed: 21549175]

22. Donahue RE, Kuramoto K, Dunbar CE. Large animal models for stem and progenitor cell analysis. Curr Protoc Immunol 2005;Chapter 22:Unit 22A 1 doi 10.1002/0471142735.im22a01s69.

23. Holland JP, Sheh Y, Lewis JS. Standardized methods for the production of high specific-activity zirconium-89. Nuclear medicine and biology 2009;36(7):729–39 doi 10.1016/j.nucmedbio.2009.05.007. [PubMed: 19720285]

24. Abou DS, Ku T, Smith-Jones PM. In vivo biodistribution and accumulation of 89Zr in mice. Nuclear medicine and biology 2011;38(5):675–81 doi 10.1016/j.nucmedbio.2010.12.011. [PubMed: 21718943]

25. Zamai L, Ahmad M, Bennett IM, Azzoni L, Alnemri ES, Perussia B. Natural killer (NK) cell-mediated cytotoxicity: differential use of TRAIL and Fas ligand by immature and mature primary human NK cells. The Journal of experimental medicine 1998;188(12):2375–80 doi 10.1084/jem.188.12.2375. [PubMed: 9858524]

26. Kayagaki N, Yamaguchi N, Nakayama M, Takeda K, Akiba H, Tsutsui H, et al. Expression and function of TNF-related apoptosis-inducing ligand on murine activated NK cells. J Immunol 1999;163(4):1906–13. [PubMed: 10438925]

27. Mestas J, Hughes CC. Of mice and not men: differences between mouse and human immunology. J Immunol 2004;172(5):2731–8 doi 10.4049/jimmunol.172.5.2731. [PubMed: 14978070]

28. Abel AM, Yang C, Thakar MS, Malarkannan S. Natural Killer Cells: Development, Maturation, and Clinical Utilization. Front Immunol 2018;9:1869 doi 10.3389/fimmu.2018.01869. [PubMed: 30150991]

29. Levy E, Reger R, Segerberg F, Lambert M, Leijonhufvud C, Baumer Y, et al. Enhanced Bone Marrow Homing of Natural Killer Cells Following mRNA Transfection With Gain-of-Function Variant CXCR4(R334X). Front Immunol 2019;10:1262 doi 10.3389/fimmu.2019.01262. [PubMed: 31231387]

30. Terren I, Mikelez I, Odriozola I, Gredilla A, Gonzalez J, Orrantia A, et al. Implication of Interleukin-12/15/18 and Ruxolitinib in the Phenotype, Proliferation, and Polyfunctionality of Human Cytokine-Preactivated Natural Killer Cells. Front Immunol 2018;9:737 doi 10.3389/fimmu.2018.00737. [PubMed: 29713323]

31. Childs RW, Carlsten M. Therapeutic approaches to enhance natural killer cell cytotoxicity against cancer: the force awakens. Nat Rev Drug Discov 2015;14(7):487–98 doi 10.1038/nrd4506. [PubMed: 26000725]

32. Somanchi SS, Senyukov VV, Denman CJ, Lee DA. Expansion, purification, and functional assessment of human peripheral blood NK cells. J Vis Exp 2011;48:e2540 doi 10.3791/2540.

33. Racanelli V, Rehermann B. The liver as an immunological organ. Hepatology 2006;43(2 Suppl 1):S54–62 doi 10.1002/hep.21060. [PubMed: 16447271]

34. Hudspeth K, Donadon M, Cimino M, Pontarini E, Tentorio P, Preti M, et al. Human liver-resident CD56(bright)/CD16(neg) NK cells are retained within hepatic sinusoids via the engagement of CCR5 and CXCR6 pathways. J Autoimmun 2016;66:40–50 doi 10.1016/j.jaut.2015.08.011. [PubMed: 26330348]

35. Bjorkstrom NK, Ljunggren HG, Michaelsson J. Emerging insights into natural killer cells in human peripheral tissues. Nat Rev Immunol 2016;16(5):310–20 doi 10.1038/nri.2016.34. [PubMed: 27121652]

36. Price TW, Greenman J, Stasiuk GJ. Current advances in ligand design for inorganic positron emission tomography tracers (68)Ga, (64)Cu, (89)Zr and (44)Sc. Dalton Trans 2016;45(40):15702–24 doi 10.1039/c5dt04706d. [PubMed: 26865360]

TRANSLATIONAL RELEVANCE

The success of adoptive immunotherapy for hematological malignancies may require infused cells to traffick to the bone marrow (BM) where malignant cells often reside. We developed a novel method to track and quantify organ distribution of adoptively transferred natural killer (NK)-cells using ^{89}Zr-oxine *ex-vivo* cell labeling and positron emission tomography (PET). Low ^{89}Zr-oxine doses required for imaging did not alter NK-cell viability or function. Following autologous infusion into rhesus macaques, labeled NK-cells were tracked for 7 days, passing through the lungs, then localizing primarily to the liver, spleen and, at low levels, the BM. No toxicity was observed, and dosimetry estimates extrapolated to humans suggested tracking could be achieved with very low radio-exposure to organs. These data suggest that ^{89}Zr-oxine-labeled NK-cell PET can be safely translated to humans for tracking distribution of adoptively infused cells and for assessing cell modification techniques to improve immune cell homing to tumor microenvironments.

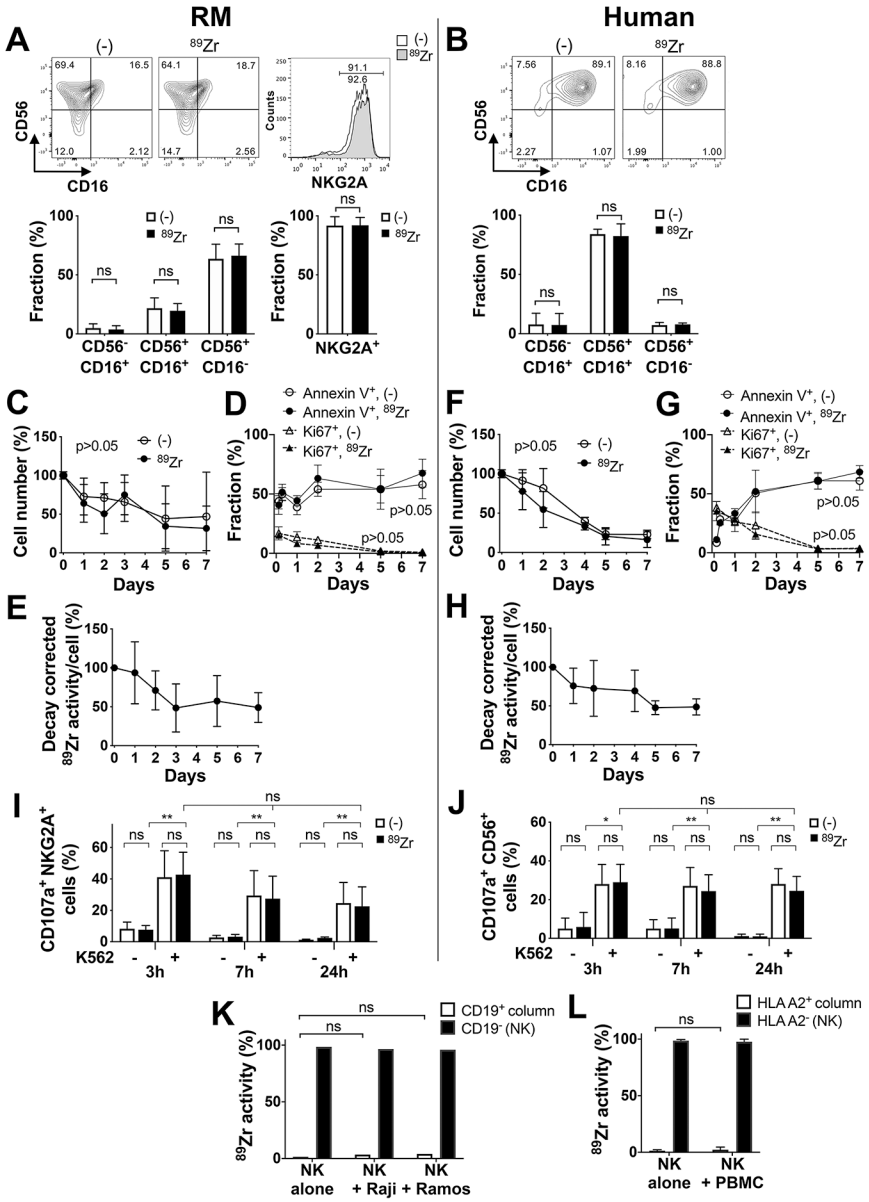

Figure 1. ^{89}Zr-oxine-labeled NK-cells have normal cellular function and do not transfer their label.

A. Flow cytometry analysis showed that the majority of *ex-vivo*-expanded RM NK-cells expressed NKG2A (n=8) and were CD56^{+}CD16^{-} (n=9), which was not altered by ^{89}Zr-oxine labeling. **B**. The majority of *ex-vivo*-expanded human NK-cells were CD56^{+}CD16^{+} (n=7), which was not altered by ^{89}Zr-labeling. **C**. RM NK-cells without (open circle) or with ^{89}Zr-oxine labeling (filled circle) showed similar viability over time when cultured in media without IL-2 (n=11). **D**. Flow cytometry analysis indicated that early after harvest from *ex-vivo* expansion cultures, a small fraction of RM NK-cells continued to proliferate (Ki67^{+}, ^{89}Zr-labeled: filled triangle, non-labled: open triangle) while annexin V^{+} apoptotic/necrotic cells increased over time (^{89}Zr-labeled: filled circle, non-labled: open circle), neither of which were impacted by ^{89}Zr-oxine labeling. **E**. Decay corrected ^{89}Zr-activity per RM NK-

cell declined at early time points and plateaued later. **F**. Similar to RM NK-cells, the number of viable human NK-cells gradually declined, with (filled circle) and without (open circle) ^{89}Zr-labeling (n=9). **G**. Human NK-cells continued to proliferate (Ki67^{+}) early after harvest from *ex-vivo* expansion cultures, regardless of ^{89}Zr-labeling, while annexin V^{+} NK-cells increased over time. **H**. ^{89}Zr-activity per human NK-cell declined over time (n=6). **I and J**. Degranulation of both RM (**I**, n=3) and human (**J**, n=3) NK-cells (cell surface CD107a) against K562 target cells, analyzed by flow cytometry, was similar regardless of ^{89}Zr-labeling 3, 7, and 24 hours after labeling (*: $p<0.05$, **: $p<0.01$, ns: $p>0.05$). **K**. ^{89}Zr-oxine-labeled human NK-cells (5×10^5 cells) were cultured alone or with CD19^{+} Raji or Ramos cells (5×10^5 cells) for 24–36 hours, then underwent CD19 positive selection. ^{89}Zr did not transfer to Raji or Ramos cells (n=3). **L**. ^{89}Zr-labeled HLA-A2 negative human NK-cells (8×10^5 cells) were cultured alone or with HLA-A2 positive PBMCs (8×10^5 cells) for 24–36 hours, then underwent HLA-A2 positive selection. ^{89}Zr did not transfer to PBMCs (n=3).

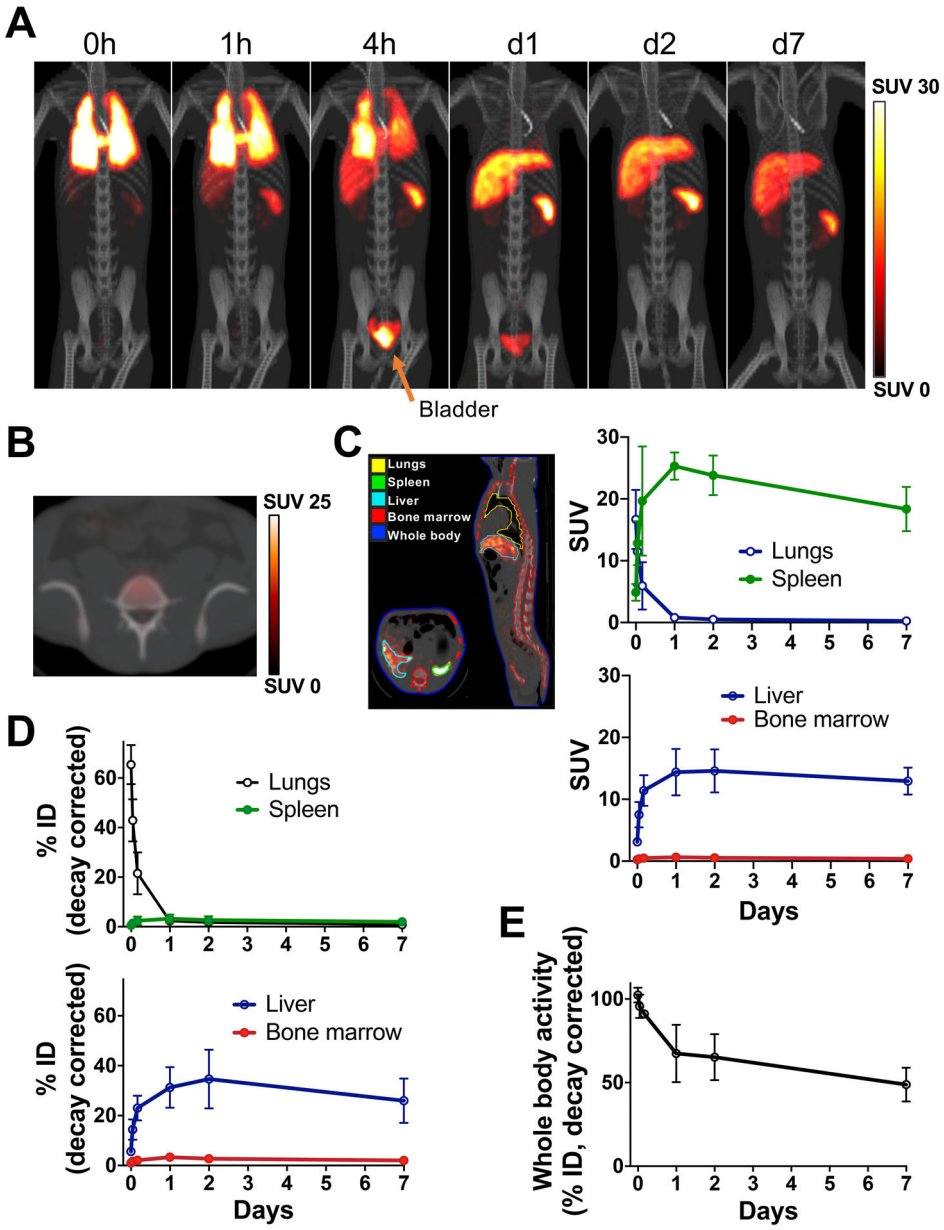

Figure 2. PET/CT imaging of autologous ^{89}Zr-oxine-labeled NK-cells enables visualization and quantitation of NK-cell trafficking after adoptive-transfer.

A. Autologous ^{89}Zr-labeled expanded NK-cells transferred to RMs were tracked by PET/CT imaging, with continuous deferoxamine infusion, for up to 7 days (n=3, 2.05 ± 0.7 MBq, 13.7± 5.2 kBq/10^6 cells, 23.5 ± 2.0×10^6 cells/kg, representative set of images). **B**. Axial PET/CT image of mid-4th lumber spine on day 1 showed minimal homing of NK-cells to the BM area of the spinal body. **C**. Kinetics of SUV values (right) obtained from images by drawing the contours on the organs (left) suggested that ^{89}Zr-labeled NK-cells migrated from the lungs to the liver and spleen. See Supplementary Fig. S2A for magnification of early time points. **D**. % ID curves indicated that most cells were in the liver while homing to the BM was limited. Also see Supplementary Fig. S2B. **E**. Whole-body activity declined

over time, indicating death of transferred ^{89}Zr-labeled cells and subsequent ^{89}Zr excretion from the body.

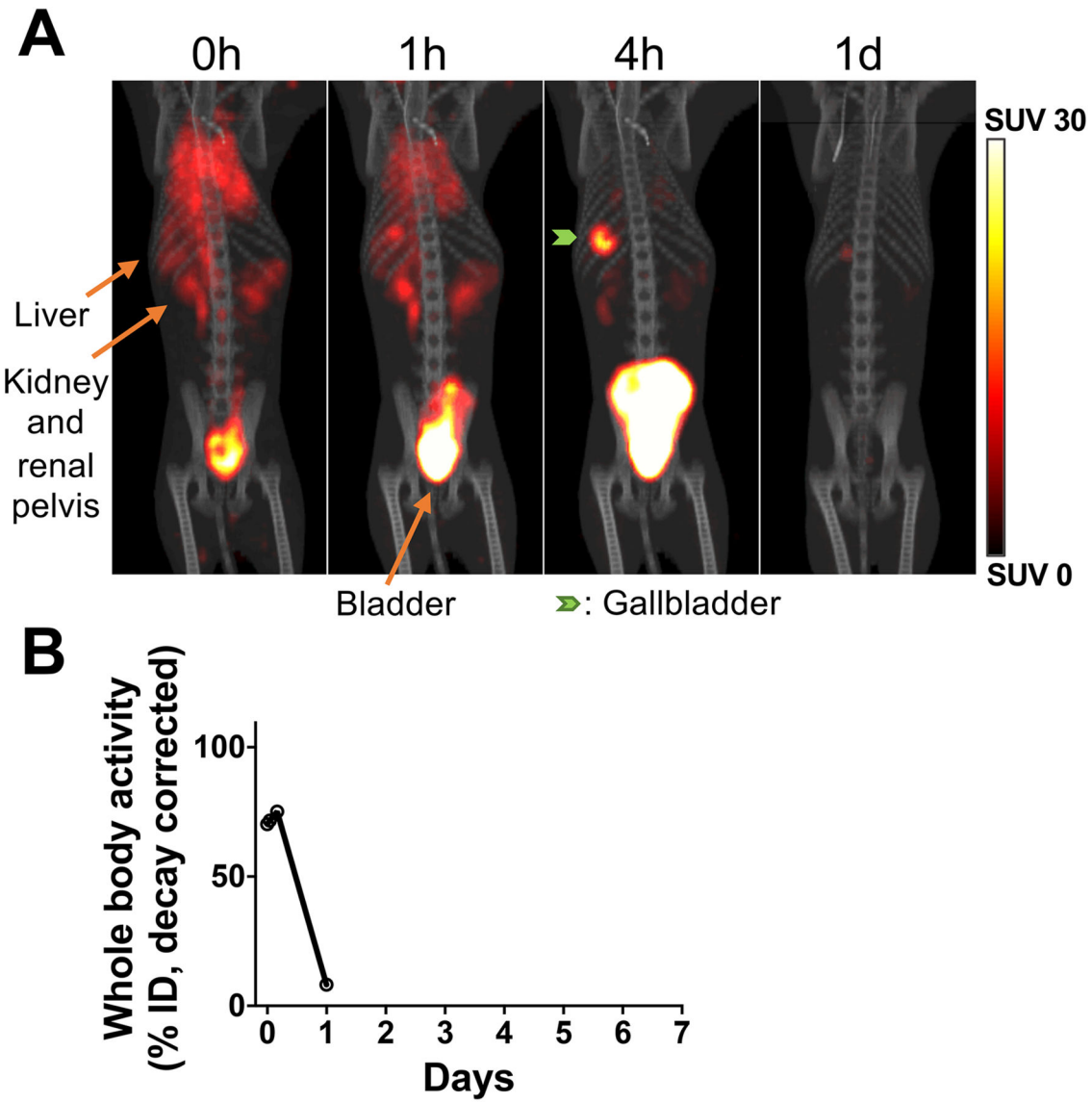

Figure 3. Deferoxamine enhances renal clearance of ^{89}Zr released from dead/dying cells.

A. ^{89}Zr-labeled apoptotic NK-cells were tracked in a RM (276 kBq, 3.5×10^6 cells/kg) by PET/CT under continuous deferoxamine infusion (n=1). ^{89}Zr released from dying/dead cells was quickly chelated by deferoxamine and excreted in the urine. By 4 hours, most of the activity was observed in the bladder. **B**. Whole-body radioactivity decreased to 8% within 1 day.

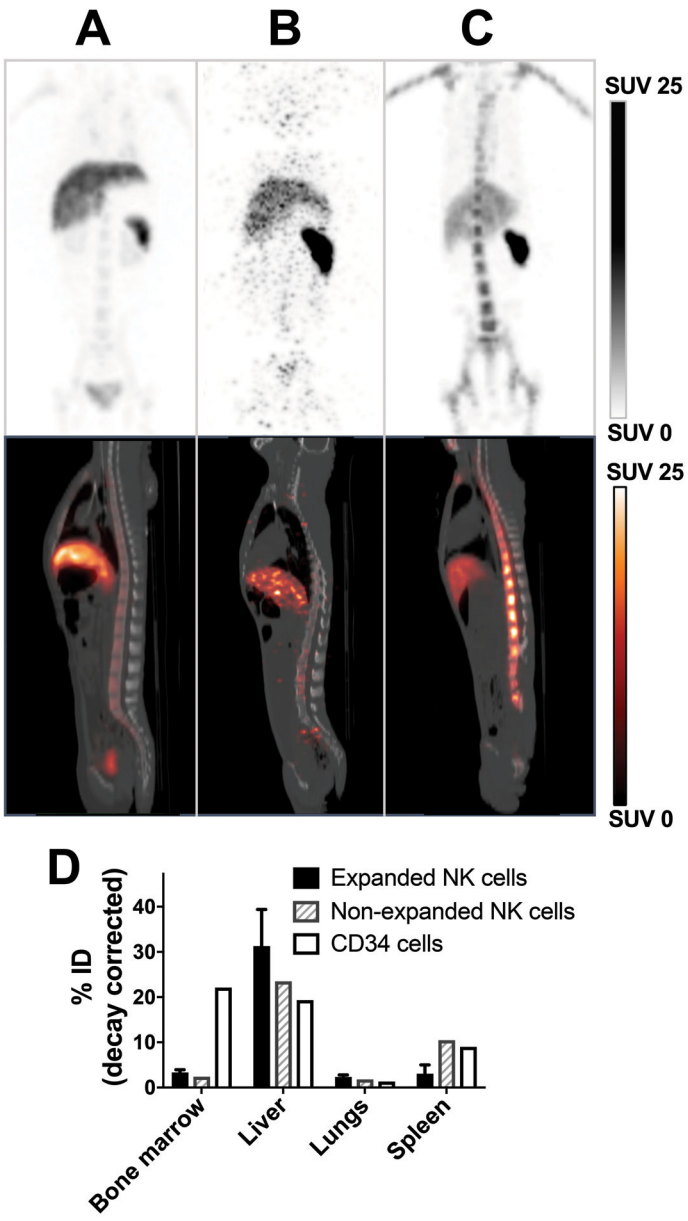

Figure 4. PET/CT imaging shows minimal homing of *ex-vivo*-expanded and non-expanded NK-cells to the BM compared to HSPCs

MIP PET (top) and sagittal PET/CT images acquired 1 day after transfer of ^{89}Zr-oxine-labeled expanded NK-cells (**A**, 2.59 MBq, 15.2 kBq/10^6 cells, 21.9×10^6 cells/kg, representative images of 3 independent experiments), non-expanded NK-cells (**B**, 185 kBq, 6.9 kBq/10^6 cells, 4.0×10^6 cells/kg, n=1) and HSPCs (**C**, 355 kBq, 44.4 kBq/10^6 cells, 1.2×10^6 cells/kg, n=1) are presented. **D**. Quantitation of the day 1 images indicated that both NK-cell populations homed to the BM far less than HSPCs. See Supplementary Fig. S3 for axial PET/CT image of mid-4th lumber spine 1 day after transfer of ^{89}Zr-oxine-labeled HSPCs and migration kinetics.

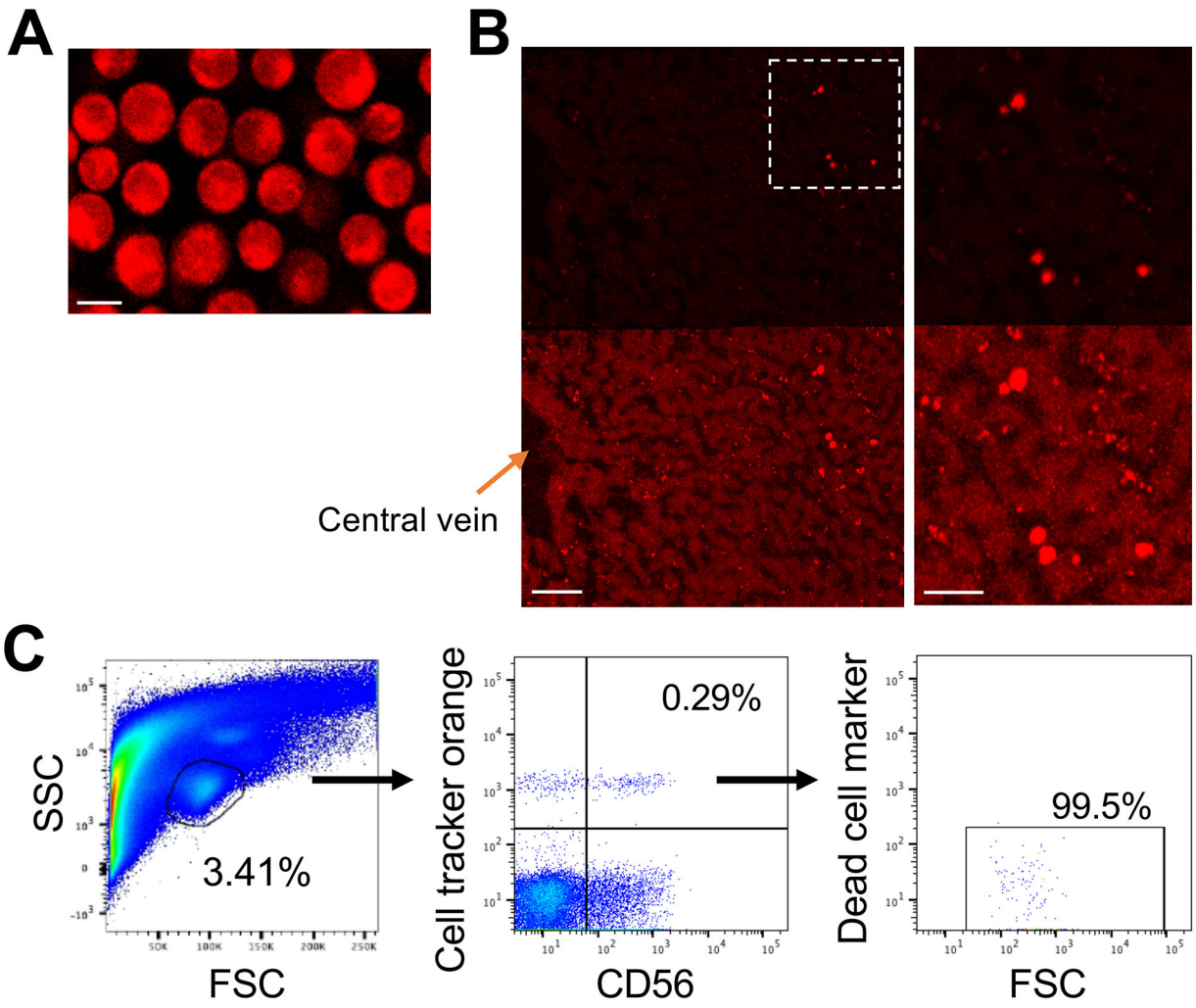

Figure 5. Biopsy confirms PET/CT imaging studies showing adoptively transferred *ex-vivo*-expanded NK-cells reside in the liver

A. Expanded NK-cells were labeled with CMRA (bar indicates 10 μm). **B**. A biopsy obtained 24 hours following adoptive-transfer (5×10^7 cells/kg) showed presence of CMRA-labeled NK-cells in the liver (representative image). Brighter images are shown at the bottom to demonstrate liver structures. The right panels show magnified views of the outlined area in the left panel. The bars indicate 100 μm (left) and 50 μm (right). **C**. Flow cytometry analysis of the biopsy samples showed the presence of viable CMRA-labeled $CD56^+$ NK-cells in the liver.

Table 1.

Human dosimetry estimates for ^{89}Zr-oxine labeled NK cells

Organs	mSv/MBq (mean ± s.d.)
Liver	3.880 ± 1.228
Lungs	1.400 ± 0.323
Red Marrow	0.319 ± 0.045
Spleen	6.240 ± 3.606
Total Body	0.317 ± 0.048
Effective Dose (mSv/MBq)	0.675 ± 0.135

1. n=3

2. Extrapolated to 70 kg adult humans.